



PUBLISHED FOR SISSA BY SPRINGER

RECEIVED: November 28, 2016

REVISED: March 3, 2017

ACCEPTED: March 9, 2017

PUBLISHED: March 24, 2017

The top right coupling in the aligned two-Higgs-doublet model

Cesar Ayala,^{a,b} Gabriel A. González-Sprinberg,^c R. Martínez^d and Jordi Vidal^a

^a*Departament de Física Teòrica, Universitat de València & Instituto de Física Corpuscular (IFIC), Centro Mixto Universitat de València-CSIC, E-46100 Burjassot, València, Spain*

^b*Department of Physics, Universidad Técnica Federico Santa María, Casilla 110-V, Valparaíso, Chile*

^c*Instituto de Física, Facultad de Ciencias, Universidad de la República, Iguá 4225, Montevideo 11600, Uruguay*

^d*Departamento de Física, Universidad Nacional de Colombia, Bogotá Distrito Capital, Colombia*

E-mail: cesar.ayala@uv.es, gabrielg@fisica.edu.uy,
remartinezm@unal.edu.co, vidal@uv.es

ABSTRACT: We compute the top quark right coupling in the aligned two-Higgs-doublet model. In the Standard Model the real part of this coupling is dominated by QCD-gluon-exchange diagram, but the imaginary part, instead, is purely electroweak at one loop. Within this model we show that values for the imaginary part of the coupling up to one order of magnitude larger than the electroweak prediction can be obtained. For the real part of the electroweak contribution we find that it can be of the order of 2×10^{-4} . We also present detailed results of the one loop analytical computation.

KEYWORDS: Beyond Standard Model, Higgs Physics

ARXIV EPRINT: [1611.07756](https://arxiv.org/abs/1611.07756)

Contents

1	Introduction	1
2	The aligned two-Higgs-doublet model	3
3	V_R top coupling in the A2HDM	5
4	Results	8
5	Conclusions	13
A	A2HDM contribution to V_R	13

1 Introduction

In 2015 the LHC center-of-mass energy has reached 13 TeV. By the end of 2016 the LHC will be close to a peak luminosity of $1.5 \times 10^{34} \text{ cm}^{-2} \text{ s}^{-1}$, with an integrated luminosity of 38 fb^{-1} . After 2020, several components of the accelerator will reach the radiation damage or reliability limit so that, by 2024 the LHC will have to be upgraded to the High-Luminosity LHC (HL-LHC), which is expected to accumulate over the next 10 years an impressive integrated luminosity of 3000 fb^{-1} at energies close to 13–14 TeV [1, 2]. The LHC is a collider designed to produce and discover new particles, in particular the Higgs boson but, in addition, it also produces a high amount of top quarks. The ATLAS and CMS experiments have already collected millions of top pairs and single top events but in this scenario of very high luminosity, they will detect billions of them in the future. Besides, next generation of colliders, such as CLIC, will eventually be built and it is expected that the top quarks physics will enter in an era of high precision.

Up to now, the only decay detected for the top quark is the weak-interaction mediated to a b quark and a W^+ boson, $t \rightarrow bW^+$. Other channels and possible departures from the Standard Model (SM) may show up in the future when new interactions will be then intensively probed in top quark physics. In order to study the properties of this weak top decay it is useful to parametrize the tbW vertex in a model independent effective approach. The most general CP-conserving and Lorentz invariant structure for this on-shell tbW vertex has four couplings: two chiral couplings, V_L and V_R , and two tensorial anomalous couplings, g_L and g_R . The left coupling V_L is the only one that it is not zero within the SM at tree level, and takes a value close to one [3]. The one-loop values of $g_{L,R}$ within the SM, the two-Higgs-doublet model (2HDM) and other extended models were recently calculated in refs. [4–6] and they will not be considered in this paper; their measurement at the LHC was investigated in ref. [7]. The top right coupling V_R was computed in the SM, at leading order, in ref. [8].

The discovery of the top quark was done at TEVATRON [9, 10] where CDF and D0 collaborations obtained a first bound on the tbW anomalous couplings [11–13] in agreement with the SM predictions. Nowadays, top quark physics is being extensively studied at LHC [14–18] where the ATLAS and CMS collaborations are looking for any signal of new physics [19–22] in their data on top decays. The study of the tbW vertex structure has been usually done by considering observables built on the measurement of the different helicity components (\pm and 0) of the W in the decay of the top quark. In recent works [23–28] it has been shown that a precise determination of the Lorentz form factors of the tbW vertex can be done with a suitable choice of observables built from longitudinal and also transverse helicities of the W coming from the top decay. The determination of other couplings of the top quark, such as the chromoelectric and chromomagnetic of the ttg (top-top-gluon) vertex has been recently studied [29] as a window for new physics, in the 2HDM-framework with a CP -violating potential. The enormous amount of collected data by the LHC (and in the future by the HL-LHC) will hopefully determine the complete structure of the tbW vertex, with a precise determination of the properties of top quark anomalous couplings to the W boson and b quark.

As already said in the previous paragraph and as it is also shown in detail in refs. [8, 30, 31], at LHC, the observables considered in the literature to bound the anomalous couplings of the tbW vertex are based on the measurement of the helicity components of the W boson product of the top decay, for $pp \rightarrow t\bar{t} \rightarrow W^+bW^-\bar{b}$ events with one (or both) of the W bosons decaying leptonically. Those observables are the F_{\pm} and F_0 fractions of W bosons produced with helicity \pm and 0 [32], respectively, angular asymmetries in the W rest frame [23, 30, 31, 33, 34], angular asymmetries in the top rest frame [23, 30, 35–38] and spin correlations [23, 30, 39, 40]. These observables are not, in general, very sensitive to the right coupling V_R . This is due to the fact that the V_R coupling has the same parity and chirality properties as the leading coupling V_L , so that the observables receive contributions from both terms on an equal footing. In ref. [8] some of these observables are redefined in such a way as to cancel the leading V_L contribution to them. Then, they are directly sensitive to V_R and can be an important tool in order to search for new physics contributions to this coupling. Based on 1.04 fb^{-1} of pp data at $s = \sqrt{7} \text{ TeV}$, with a combined analysis of the W helicity fractions F_0 and F_L , for single-lepton and dilepton events, and angular asymmetries, A_+ and A_- , for single-lepton channels [41], the direct bound on the Wtb right coupling obtained is [3]

$$-0.20 < V_R < 0.23. \quad (1.1)$$

On the other hand, the current 95% C.L. bound on V_R from the precise measurement of the radiative B -meson decay $\bar{B} \rightarrow X_s \gamma$, is [42]

$$-0.0007 < V_R < 0.0025, \quad (1.2)$$

so that a combined analysis of collider data with these precise measurement of B -meson decay may be useful to bound the V_R top coupling.

A simple and widely studied extension of the electroweak theory is to consider a second scalar doublet added to the SM [43, 44]. However, tree level flavour changing neutral

currents (FCNC) arise unless new hypothesis are introduced. A recent proposal in order to address this issue is the aligned two Higgs doublet model A2HDM [45], where the two Yukawa matrices coupled to the same type of right-handed fermion are aligned in flavour space. Then, no FCNCs appear at tree level. Besides, most of the popular versions of the 2HDM are reproduced with particular choices of the A2HDM parameters. In this paper we present a detailed calculation of the new contributions to the V_R top right coupling in the general framework of the A2HDM.

This work is organized as follows. In the next section we briefly review the A2HDM, introducing the notation used in the paper and presenting the current limits that constraint the parameters of the model. In section 3 we define the vertex parametrization and show the details of the computation of the different contributions to the right vector coupling V_R within the A2HDM. In section 4 we investigate the sensitivity of the V_R coupling to the scalar mixing angle and alignments parameters, for a CP-conserving scalar potential. We show the results obtained for values of the parameters and masses of the new particles so as to cover the meaningful parameter space. The results for 2HDM Type-I and II are also shown. We present our conclusions in section 5.

2 The aligned two-Higgs-doublet model

The 2HDM extends the SM by adding a second scalar doublet $\phi_2(x)$ with the same hypercharge $Y = 1/2$ [43, 44]. Similarly to what happens in the SM, after symmetry breaking, the neutral components of the two doublets get non zero vacuum expectation values $\langle \phi_i \rangle_{i=1,2}^T = (0, \frac{v_i}{\sqrt{2}} e^{i\theta_i})$.

The so called Higgs basis $(\Phi_1(x), \Phi_2(x))$ is obtained through a rotation of the $\phi_1(x), \phi_2(x)$ states given by the angle β (defined as $\tan \beta = \frac{v_2}{v_1}$), in such a way that only one of the doublets $(\Phi_1(x))$ gets a non-zero expectation value $v = \sqrt{v_1^2 + v_2^2}$.

In this basis, the three components of the doublets can be written as:

$$\Phi_1(x) = \begin{pmatrix} G^+(x) \\ \frac{1}{\sqrt{2}} (v + S_1(x) + i G^0(x)) \end{pmatrix}, \quad \Phi_2(x) = \begin{pmatrix} H^+(x) \\ \frac{1}{\sqrt{2}} (S_2(x) + i S_3(x)) \end{pmatrix} \quad (2.1)$$

where $G^0(x)$ and $G^\pm(x)$ correspond to the three would-be Goldstone bosons of the SM, $H^\pm(x)$ are two new charged scalar fields and $\{S_i(x)\}_{i=1,2,3}$ are three neutral scalars with no defined mass. To get the three mass eigenstates as a linear combination of the later three scalars one has to perform an orthogonal transformation \mathcal{R} so that the new three mass eigenstates, $\{\varphi_i(x)\}_{i=1,2,3} = \{h(x), H(x), A(x)\}$, can be written as:

$$\varphi_i(x) = \mathcal{R}_{ij} S_j(x); \quad i, j = 1, 2, 3. \quad (2.2)$$

The particular form of the potential will define the matrix \mathcal{R} and the structure of the scalar mass matrix and mass eigenstates. If the potential is CP-conserving, the CP-even states

$\{S_1(x), S_2(x)\}$ will not mix with the CP-odd one ($S_3(x)$) so that:

$$\begin{aligned} H(x) &= \cos \gamma S_1(x) + \sin \gamma S_2(x) \\ h(x) &= -\sin \gamma S_1(x) + \cos \gamma S_2(x) \\ A(x) &= S_3(x) \end{aligned} \tag{2.3}$$

where γ is the neutral scalar mixing angle.

The most general Yukawa Lagrangian, with standard fermionic content, will have different couplings to $\Phi_1(x)$ and $\Phi_2(x)$ doublets. It means that when one diagonalizes the fermionic mass matrices -in the Higgs basis- this transformation will no diagonalize the fermion-scalar Yukawa matrices. The Yukawa lagrangian can then be written as:

$$\begin{aligned} \mathcal{L}_Y &= -\frac{\sqrt{2}}{v} \left\{ \bar{Q}_L(x) [\mathcal{M}_d \Phi_1(x) + \mathcal{Y}_d \Phi_2(x)] d'_R(x) \right. \\ &+ \bar{Q}_L(x) [\mathcal{M}_u \tilde{\Phi}_1(x) + \mathcal{Y}_u \tilde{\Phi}_2(x)] u'_R(x) \\ &\left. + \bar{L}_L(x) [\mathcal{M}_l \Phi_1(x) + \mathcal{Y}_l \Phi_2(x)] l'_R(x) + \text{h.c.} \right\}, \end{aligned} \tag{2.4}$$

where $\tilde{\Phi}_i(x) = i\tau_2 \Phi_i^*(x)$, all fermionic fields, $Q_L(x)$, $L_L(x)$, $d'_R(x)$, $u'_L(x)$ and $l'_R(x)$, are three-dimensional vectors in the flavour space, \mathcal{M}_f ($f = d, u, l$) are the non-diagonal 3×3 fermion mass matrices, and \mathcal{Y}_f are the fermion-scalar Yukawa couplings that are, in general, also non-diagonal. The rotation to the fermionic mass eigenstates ($d(x)$, $u(x)$, $l(x)$, $\nu(x)$) which diagonalizes the mass matrices \mathcal{M}_f will, in general, not diagonalize simultaneously the Yukawa matrices \mathcal{Y}_f , so that they will introduce FCNC at tree level. Among the different approaches to avoid this unwanted effect we choose the one that, before diagonalization, makes both Yukawa matrices $-\mathcal{M}_f$ and \mathcal{Y}_f , for each type of right handed fermions- proportional to each other (alignment in the flavour space). Then, they can be simultaneously diagonalized and the diagonal Yukawa matrices satisfy the relations:

$$Y_j = \varsigma_j M_j, \quad i = d, l \quad Y_u = \varsigma_u M_u, \quad \varsigma_f^* = \frac{\xi_f - \tan \beta}{1 + \xi_f \tan \beta}, \quad f = u, d, l \tag{2.5}$$

with ξ_f being an arbitrary complex number and M_f ($f \equiv u, d, l$) diagonal mass matrices. This is the so called A2HDM. For different values of the ξ_f parameter (see [45]) it reproduces the 2HDM with discrete Z_2 symmetries, Type-I, II, X, Y and inert model. Obviously if the ς_f are taken to be arbitrary complex numbers the Lagrangian incorporate new sources of CP-violation.

The Yukawa lagrangian can be then written as:

$$\begin{aligned} \mathcal{L}_Y &= -\frac{\sqrt{2}}{v} H^+(x) \bar{u}(x) [\varsigma_d V M_d P_R - \varsigma_u M_u V P_L] d(x) \\ &- \frac{\sqrt{2}}{v} H^+(x) \varsigma_l \bar{\nu}(x) M_l P_R l(x) \\ &- \frac{1}{v} \sum_{i,f} \varphi_i(x) y_f^{\varphi_i} \bar{f}(x) M_f P_R f(x) + \text{h.c.}, \end{aligned} \tag{2.6}$$

where V is the Cabibbo-Kobayashi-Maskawa matrix and $P_{R,L} \equiv \frac{1}{2}(1 \pm \gamma_5)$ are the chirality projectors.

The neutral Yukawa terms are flavour-diagonal and the couplings $y_f^{\varphi_i}$ ($\varphi_i = h, H, A$) are proportional to the corresponding elements of the neutral scalar mixing matrix \mathcal{R} :

$$\begin{aligned} y_{d,l}^{\varphi_i} &= \mathcal{R}_{i1} + (\mathcal{R}_{i2} + i\mathcal{R}_{i3}) \varsigma_{d,l}, \\ y_u^{\varphi_i} &= \mathcal{R}_{i1} + (\mathcal{R}_{i2} - i\mathcal{R}_{i3}) \varsigma_u^*. \end{aligned} \tag{2.7}$$

In the particular case of a CP-conserving potential they can be written as:

$$\begin{aligned} y_{d,l}^H &= \cos \gamma + \sin \gamma \varsigma_{d,l}, & y_u^H &= \cos \gamma + \sin \gamma \varsigma_u^*, \\ y_{d,l}^h &= -\sin \gamma + \cos \gamma \varsigma_{d,l}, & y_u^h &= -\sin \gamma + \cos \gamma \varsigma_u^*, \\ y_{d,l}^A &= i \varsigma_{d,l}, & y_u^A &= -i \varsigma_u^*. \end{aligned} \tag{2.8}$$

Then, the CP-conserving A2HDM contains 10 real parameters: the three complex alignment constants $\varsigma_{u,d,l}$, the three scalar masses m_{A,H,H^\pm} , and the scalar mixing angle γ . We will assume that the light CP-even Higgs h is the SM-like Higgs with a mass of 125.09 GeV [3]. The other parameters have not yet been measured and they can be constrained by indirect phenomenological and theoretical arguments.

The presence of a charged Higgs is a signature of the model that allows some constraints coming from the associated phenomenology. In ref. [46] combined bounds on $\varsigma_{u,d,l}$ and m_{H^\pm} are obtained from: a) tau decays, $|\varsigma_l|/m_{H^\pm} \leq 0.40 \text{ GeV}^{-1}$, and b) a global fit to the tree leptonic and semi-leptonic decays of pseudoscalar mesons, $|\varsigma_u \varsigma_l^*|/m_{H^\pm}^2 \lesssim 0.01 \text{ GeV}^{-2}$ and $|\varsigma_d \varsigma_l^*|/m_{H^\pm}^2 \lesssim 0.1 \text{ GeV}^{-2}$. Bounds can be improved by looking at loop-induced processes, $Z \rightarrow b\bar{b}$, $B^0-\bar{B}^0$ and $K^0-\bar{K}^0$ mixing, and $\bar{B} \rightarrow X_s \gamma$, assuming that the dominant new-physics corrections to the observables are those generated by the charged scalar; then $|\varsigma_u| < 1.91$ for $m_{H^\pm} = 500 \text{ GeV}$ [46, 47].

Bounds on ς_d are more difficult to get from phenomenology so an upper bound as big as $|\varsigma_d| \leq 50$ can be used [47]. Studies of the radiative decays $\bar{B} \rightarrow X_{s,d} \gamma$, show that the combination $|\varsigma_u^* \varsigma_d|$ is strongly correlated with the mass of the scalar charged boson m_{H^\pm} , thus one find that $|\varsigma_u^* \varsigma_d| \leq 25$ for $m_{H^\pm} \in (100, 500) \text{ GeV}$ [46, 47]. More constraints on the ς_u - ς_d plane can also be set from \bar{B} decays and are given in refs. [46, 47]

Recently, direct searches of light charged scalar Higgs in $t \rightarrow H^+ b$ decay in ATLAS and CMS [48] give an upper bound [49] on the combination $|\varsigma_u^* \varsigma_d|$ that excludes part of the allowed regions constrained by \bar{B} decays.

All these limits put constraints on the parameter space of the model. In this paper we only consider the ones that are related to the top physics.

3 V_R top coupling in the A2HDM

The most general Lorentz structure of the amplitude \mathcal{M}_{tbW} , for on-shell particles, in the $t(p) \rightarrow b(p')W^+(q)$ decay is:

$$\begin{aligned} \mathcal{M}_{tbW} &= -\frac{e}{\sin \theta_w \sqrt{2}} \epsilon^{\mu*} \times \\ &\bar{u}_b(p') \left[\gamma_\mu (V_L P_L + V_R P_R) + \frac{i\sigma_{\mu\nu} q^\nu}{m_W} (g_L P_L + g_R P_R) \right] u_t(p), \end{aligned} \tag{3.1}$$

where the outgoing W^+ momentum, mass and polarization vector are $q = p - p'$, m_W and ϵ^μ , respectively. The couplings are all dimensionless; V_L and V_R parameterize the left and right vector couplings while g_L and g_R are the so called left and right anomalous tensor couplings, respectively.

In an effective Lagrangian approach these couplings arise as contributions at low energy of non-renormalizable lagrangian terms, originated in a high energy theory. This approach assumes that the new physics spectrum is well above the electroweak (EW) energy scale [32, 50, 51].

The couplings V_R , g_R and g_L are zero at tree level within the SM, and V_L is given by the Kobayashi-Maskawa matrix element $V_L = V_{tb} \simeq 1$ [3]. The values of the anomalous tensor couplings at one loop have been calculated in ref. [4] for the SM, and in ref. [5] for a general A2HDM.

The SM contribution to V_R has been calculated in ref. [8]. There, the QCD one loop gluon exchange and the one loop contribution from the EW sector of the SM have been explicitly calculated. For the central values of the standard masses and couplings given in ref. [3], they are:

$$V_R(\text{QCD}) = 2.68 \times 10^{-3}, \quad V_R(\text{EW}) = (-0.018 + 8.92 i) \times 10^{-5}. \quad (3.2)$$

We would like to call the attention of the reader to the fact that, as can be seen from ref. [8], the EW contribution to the real part of the V_R coupling, from most of the EW diagrams considered there, is of the order of 10^{-5} but, due to accidental cancellations among them, the final result is two orders of magnitude smaller. We also found that these cancellations are very sensitive to values of the SM parameters used in the calculation in such a way that the final result for $\text{Re}[V_R(\text{EW})]$ is strongly dependent on small changes (within experimental errors given in ref. [3]) on the SM masses and couplings. Thus, for example, we see that the value for the real part of the coupling moves from $+0.091 \times 10^{-5}$ to -0.115×10^{-5} , when m_t runs over its PDG-allowed range ($m_t = (173.21 \pm 0.87)$ GeV), showing that it remains (in that sense) undetermined. Only a global bound, $|\text{Re}[V_R(\text{EW})]| \lesssim 10^{-6}$, can be set when considering the uncertainties of the present SM data. The value shown in eq. (3.2) is the one we obtain using the central values (given by PDG. [3]) for the SM parameters and it is given just as a reference value for the SM-EW prediction in this work (SM-EW central value). The imaginary part instead, remains stable, of the order of 10^{-5} , and it is purely EW.

In the 2HDM, the couplings structure of the tbW remains unchanged at tree level. However, at one loop, in addition to the usual particle contents of the SM, the three new neutral scalars h , H and A , and the new charged scalars H^\pm of the 2HDM may circulate in the internal lines of the loop and new contributions to the V_R coupling arise. The structure of the one loop diagrams contributing to the V_R top right-coupling is given in figure 1.

We denote each diagram by the label ABC according with the particles running in the loop. In table 1 we shown the 17 new diagrams to be considered, ordered by the position (A, B, or C) of the neutral scalars φ_i , where φ_i stands for one of the neutrals h , H and A in the diagram types from (1) to (3), while for diagrams types (4) to (7), φ_i runs only for the neutral scalar bosons h and H . It is important to notice that diagrams type (5)

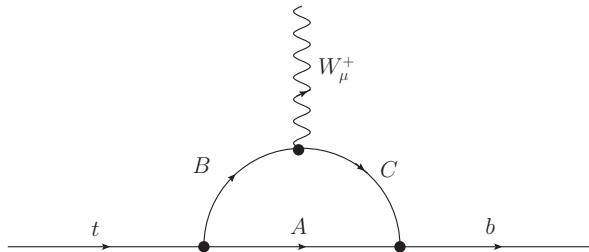


Figure 1. One-loop contributions to the V_R coupling in the $t \rightarrow bW^+$ vertex.

Type	Particles in the loop ABC	
(1)	$t \varphi_i H^-$	$\varphi_i = h, H, A$
(2)	$b H^+ \varphi_i$	
(3)	$\varphi_i t b$	
(4)	$t \varphi_i W^-$	$\varphi_i = h, H$
(5)	$b W^+ \varphi_i$	
(6)	$t \varphi_i G^-$	
(7)	$b G^+ \varphi_i$	

Table 1. Classification of the new the Feynman diagrams by the particles circulating in the loop.

and (7) always have an imaginary part while, depending on the mass of the new scalar charged Higgs (H^\pm), diagrams type (2) may or may not develop it.

Chirality imposes that all the contributions are proportional to the bottom mass and can be written as:

$$V_R^{ABC} = \alpha V_{tb} r_b I^{ABC}, \quad (3.3)$$

where $r_b = m_b/m_t$ and I^{ABC} is the Feynman integral corresponding to the given diagram. In appendix A we give the analytical expressions of all these integrals, for the diagrams shown in table 1.

The V_R coupling depends on the scalar mixing angle γ and on the alignment parameters ς_u and ς_d . The mass dependence is parameterized by the dimensionless variable $r_X = m_X/m_t$, where m_X is the mass of the particle X circulating in the loop. For the neutral scalar masses above the TeV scale, the Feynman integrals give negligible values when compared to the SM contributions. However, the V_R coupling is very sensitive to the new particles masses when they take lower values.

As in the SM, some of the diagrams are ultraviolet divergent, but we know that the total result must be finite. In appendix A it can be seen that the sum of diagrams (3), (6) and (7), to the SM diagrams $G^0 t b$, $t G^0 G^-$ and $b G^+ G^0$, respectively, cancel all the ultraviolet divergences and the total result is finite. This fact has been also used as a test of our analytical calculation.¹

¹The logarithmic terms in the expressions given in appendix A are the finite contributions coming from the sum of the divergent part of each of the diagrams evaluated.





Scalar mass scenarios (in GeV)					Type of line and color
	m_h	m_H	m_A	m_{H^\pm}	
I	125.09	170	150	320	
Ii	125.09	170	150	150	
II	125.09	866	866	320	
III	125.09	866	866	150	

Table 2. Different scalar mass scenarios taken for the analysis. Each scenario is identified by a different color and type of line in the plots.

We recover the SM expressions from the A2HDM just by taking the $\varsigma_{u,d} \rightarrow 0$ limit and setting $\gamma = -\pi/2$, in such a way that the neutral scalar h has the same couplings as the SM Higgs boson. In that limit we explicitly checked that the contributions to the top right-coupling in the A2HDM — diagrams type (3) to (7) — are identical to the corresponding ones in the SM obtained in ref. [8].

4 Results

In this section we present the one loop corrections to the top right-coupling V_R in the A2HDM. As already stated, these corrections depend on the alignment parameters $\varsigma_{u,d}$, the scalar mixing angle γ and on the masses of the new particles: 2 neutrals scalars h and H , one axial A , and two charged scalars H^\pm . We write the alignment parameters as:

$$\varsigma_u = \rho_u e^{i\theta_u}, \quad \varsigma_d = \rho_d e^{i\theta_d}, \quad (4.1)$$

and we investigate separately the effects of modulus and phases on V_R . In addition to the masses of the new particles we have five free parameters: ρ_u , ρ_d , θ_u , θ_d and the mixing angle γ .

We chose different sets of values for the masses of the new neutral and charged scalar particles; the scenarios we consider are shown in table 2. The new scalar masses are taken to be of the order of 10^2 GeV [3, 52, 53]. In the framework of 2HDM and under certain assumptions on its dominant decays, the charged scalar mass, m_{H^\pm} , is excluded to be below 85 GeV by LEP data [54]. Then, it can take values below the top quark mass, so that the decay $t \rightarrow bH^\pm$ is kinematically possible and therefore, type (2) diagrams may develop an absorptive part. These scenarios are called (i) in our paper and we fix for them the mass of the charged scalar, m_{H^\pm} , to be 150 GeV. For the other cases, where $m_{H^\pm} > m_t$, we take $m_{H^\pm} = 320$ GeV, as shown in table 2. In addition, for a CP conserving scalar potential [55] we have to impose that $m_h \leq m_H$. We define four different mass scenarios: two with three light neutral scalars (I and Ii) and two with h as the only light scalar (II and III). The other possible two, with the CP-odd scalar A being the lightest one, are disfavored by present LHC data [56, 57] and are not considered here.

The set of scenarios given in table 2 allows us to investigate the whole meaningful parameter space and to determine the regions where V_R strongly differs from the SM-EW

prediction. In all scenarios the value of the heaviest (scalar or pseudoscalar particle) mass, 866 GeV, is fixed by setting $r_{\text{heaviest}} = (m_{\text{heaviest}})/m_t = 5$.

For our numerical analysis we define Q_V^{Im} as the ratio of the imaginary part of the V_R coupling in the A2HDM to the SM-EW:

$$Q_V^{\text{Im}} \equiv \frac{\text{Im}(V_R^{\text{A2HDM}})}{\text{Im}(V_R^{\text{EW}})}. \quad (4.2)$$

Regarding the analysis of the V_R real part, due to the uncertainty already commented in the SM-EW, we present the results for the A2HDM in terms of $\text{Re}(V_R) = V_R^{\text{Re}}$.

For the different mass scenarios defined in table 2, we study the V_R dependence on the four alignment parameters $\rho_{d,u}$, $\theta_{u,d}$, and on the scalar mixing angle γ . We show the results for conservative values of the modulus, i.e. for $\rho_{u,d} \sim 1$. Larger values of these modulus will certainly produce large deviations from the SM predictions but these values are disfavoured with present data [46, 47].

In figure 2 we show the dependence of V_R^{Re} on the γ mixing angle, for different values of the θ_u parameter, with $\rho_{u,d} = 1$ and fixing $\theta_d = \pi/4$. V_R^{Re} in the A2HDM can be three orders of magnitude bigger than the SM-EW central prediction, given by eq. (3.2), for scenarios II and IIIi, while it can be only one order of magnitude larger for scenarios I and Ii. The behaviour with the γ parameter always exhibits the usual oscillating dependence. We checked that these results do not crucially depend on the particular choice of θ_d . Similar values -with a slight shift of the central values of the V_R coupling- are found when fixing $\theta_u = \pi/4$ and varying θ_d .

In figure 3 we show the behaviour of Q_V^{Im} for the same set of parameters as given in figure 2. For $\rho_{u,d} = 1$, $\theta_d = \pi/4$, and θ_u given in the plots, it can be up to three times larger than the SM-EW central value, as can be seen in the third plot of figure 3 (scenarios II and IIIi). For scenarios I and Ii, the deviation from the SM-EW central value is much smaller. The figures show the expected dependence of the observable with γ as a combination of $\sin \gamma$ and $\cos \gamma$. As in the real part of the coupling, the plots for $\text{Im}(V_R)$ present similar behaviour as the one shown in figure 3, with a small shift of their central values, when interchanging $\theta_u \leftrightarrow \theta_d$.

The V_R coupling is more sensitive to the values of ρ_u than to those of ρ_d . The last one may move over a wide range of values ($1 < \rho_d < 10$) without crucially changing the results. In the following we fix the values of the $\rho_d = 1$ and $\theta_d = \pi/4$ as a representative choice of these parameters and we study the dependence of V_R with the rest of the parameters of the model.

In figure 4 we show V_R (real and imaginary parts) as functions of the θ_u angle, for the scalar mixing angle $\gamma = \pi/4$. As seen there, the real part can be three (two) orders of magnitude bigger than the SM-EW central one for scenarios II and IIIi (I and Ii), while the imaginary part can take values up to three times larger than the SM-EW central value prediction, for scenarios II and IIIi.

In figure 5 we present the dependence of V_R on the coupling parameter ρ_u . The plots show that V_R^{Re} is three (two) orders of magnitude larger than the SM-EW central value, for scenarios II and IIIi (I and Ii). Besides, for large values of the ρ_u parameter, V_R^{Re} grows

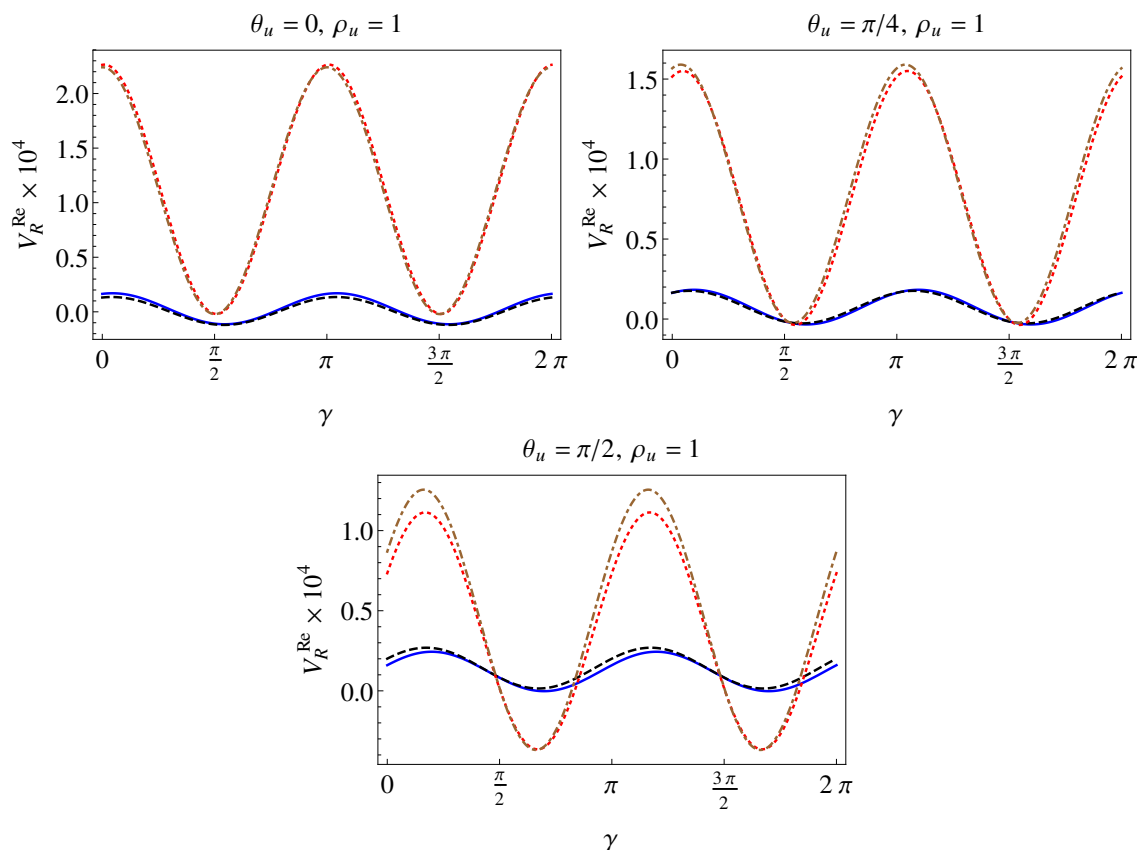


Figure 2. $V_R^{\text{Re}} = \text{Re}(V_R^{\text{A2HDM}})$, as a function of the γ scalar mixing angle, for different θ_u values and $\rho_{u,d} = 1$, $\theta_d = \pi/4$.

Model	ς_d	ς_u
Type-I	$\cot \beta$	$\cot \beta$
Type-II	$-\tan \beta$	$\cot \beta$

Table 3. Values for $\varsigma_{u,d}$ that reproduce the Type-I and Type-II 2HDM.

with ρ_u independently of the values of the other parameters of the model, such as γ and θ_u . A similar behaviour is found for the imaginary part of V_R , that can be a factor seven larger than the SM-EW central prediction for large values of ρ_u .

Finally, we compute V_R for Type-I [58, 59] and Type-II [59, 60] 2HDM.² In table 3 we show the $\varsigma_{u,d}$ values that reproduce the Type-I and Type-II models.

For Type-I and Type-II 2HDM, we present the results as a function of $\tan \beta$, for the different mass scenarios considered. We work on the alignment limit, $\gamma = -\pi/2$, where the neutral scalar h has SM-like couplings to the photon and to the weak bosons. The results for the real part of V_R are shown in figure 6. For Type-I model, V_R takes values one order of magnitude larger than the SM-EW central one, for $1 < \tan \beta < 4$ and for all mass scenarios; for $\tan \beta \gg 4$ it rapidly decreases. Note that for Type-I 2HDM the Yukawa

²See ref. [61] for a study of the values of the different top couplings in Type-I and Type-II 2HDM.

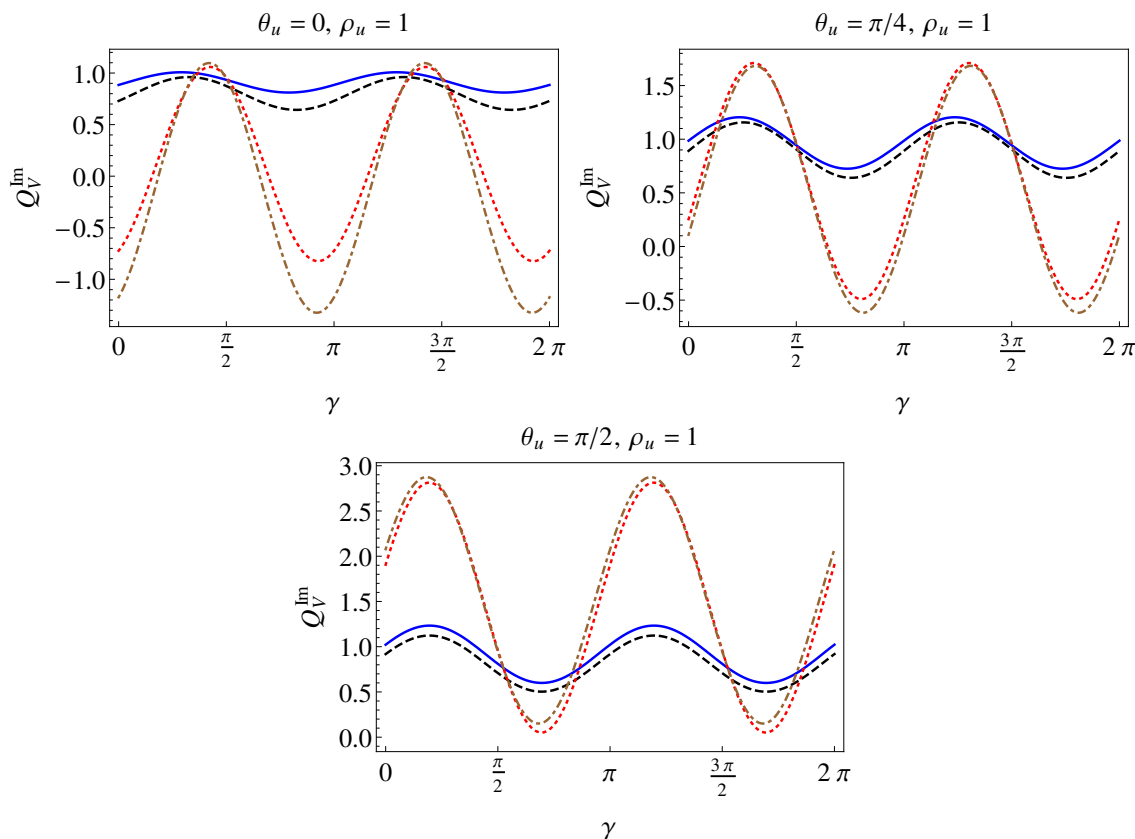


Figure 3. Q_V^{Im} (eq. (4.2)) dependence with the γ scalar mixing angle, for different θ_u values and for $\rho_{u,d} = 1$, $\theta_d = \pi/4$.

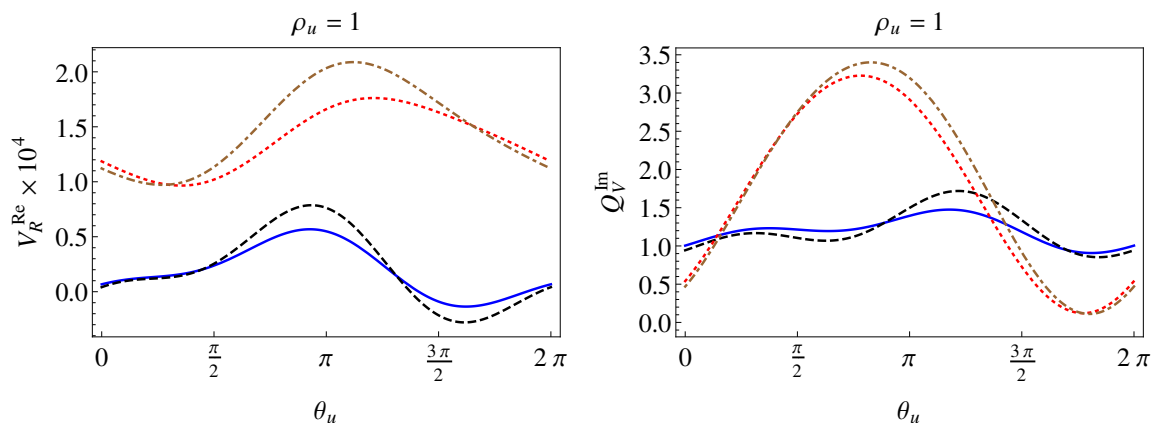


Figure 4. $V_R^{\text{Re}} = \text{Re}(V_R^{\text{A2HDM}})$ and Q_V^{Im} as function of the θ_u parameter, with $\gamma = \pi/4$, $\rho_d = 1$ and $\theta_d = \pi/4$.

couplings go to zero in the large $\tan \beta$ limit. For Type-II model the value of V_R grows with $\tan \beta$, reaching values close to 10^{-4} (10^{-5}) for $\tan \beta \simeq 50$ in the mass scenarios I and II (II and III). We also find that, within these models, V_R^{Im} is very close to the SM-EW value and almost constant for the considered mass scenarios.

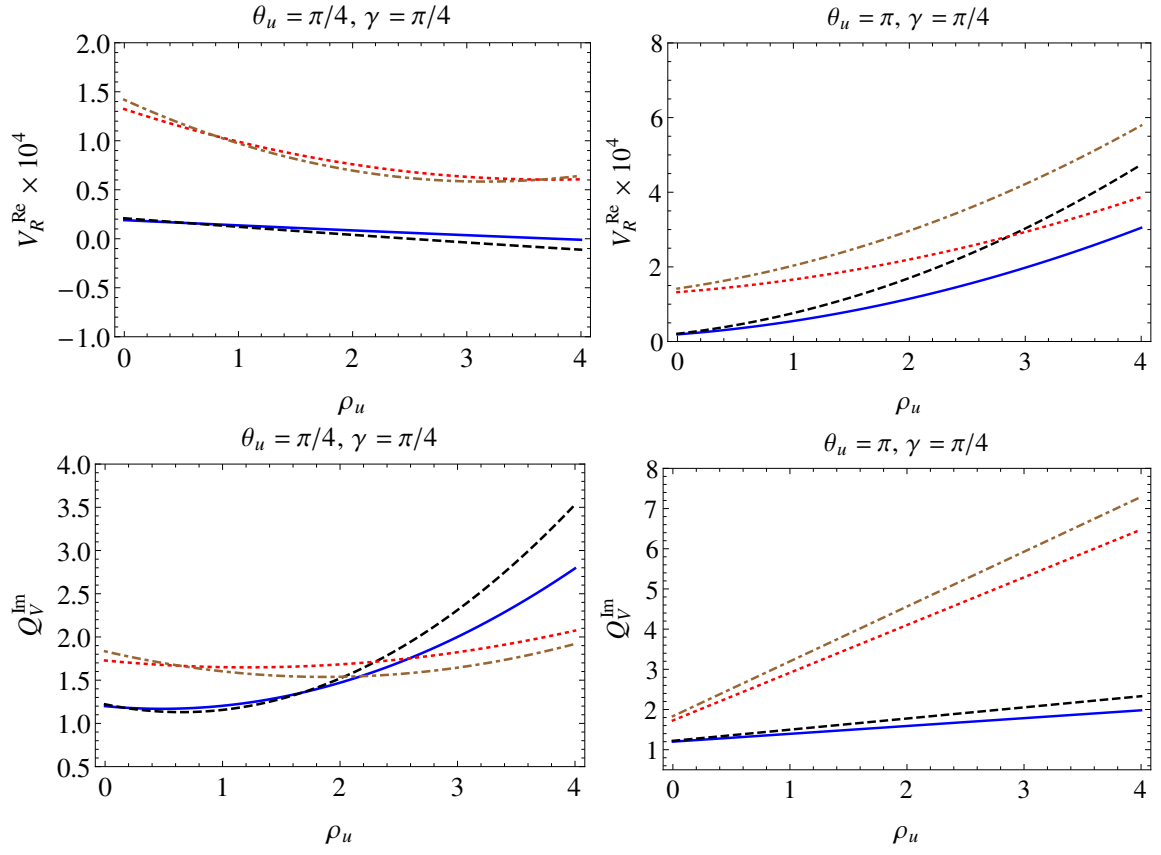


Figure 5. $V_R^{\text{Re}} = \text{Re}(V_R^{\text{A2HDM}})$ and Q_V^{Im} as a function of ρ_u for values of θ_u given in the plots and for fixed values $\gamma = \pi/4, \rho_d = 1$ and $\theta_d = \pi/4$.

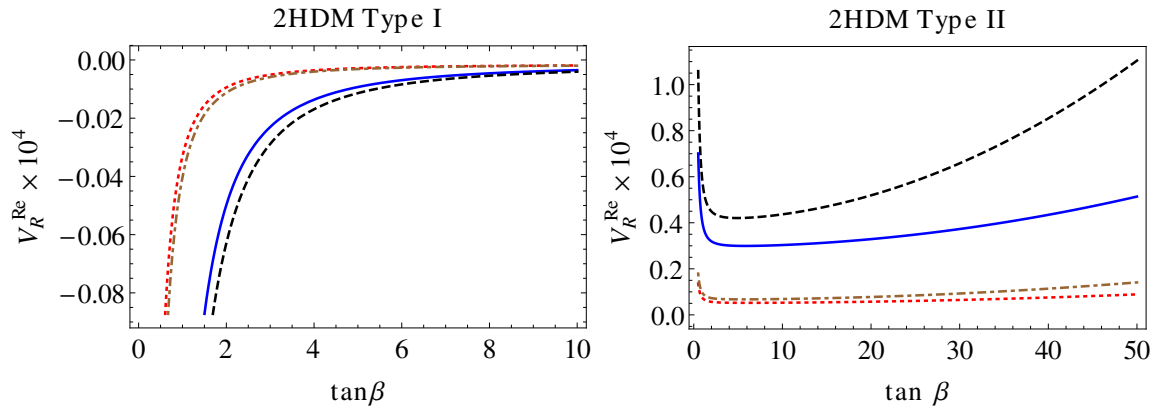


Figure 6. Type-I 2HDM prediction for V_R^{Re} (left) and Q_V^{Im} (right) as a function of $\tan \beta$, with $\gamma = -\pi/2$.

5 Conclusions

We computed the one-loop contribution to V_R in the A2HDM. In the SM, accidental cancellation among the one loop EW parts results in values for V_R^{Re} two orders of magnitude smaller than expected from each diagram. This cancellation does not take place in the A2HDM. Then, depending on the values for the parameters of the model, the magnitude of V_R^{Re} can be up to 10^{-3} and close to the leading QCD contribution. V_R^{Im} can be one order of magnitude larger than the SM prediction for $\rho_{u,d} > 4$ but, for $\rho_{u,d} \sim 1$, its magnitude is a few times larger. For Type-II (Type-I) 2HDM, V_R^{Re} can grow up to 10^{-4} (10^{-5}), for $\tan\beta \approx 10$ and depending of the mass scenarios considered, while the imaginary part remains basically of the same order as in the SM-EW.

For the HL-LHC with a high top statistic, the sensitivity to the V_R coupling will be improved by at least two orders of magnitude. In addition, with the new generation of High Luminosity Super B Factories [62], the current bound on V_R from radiative B -meson decay is expected to be improved at least in a few percent. Then the A2HDM prediction for V_R is expected to be very close to be observable.

Acknowledgments

This work has been supported, in part, by the Ministerio de Economía y Competitividad (MINECO), Spain, under grants FPA2014-54459-P and SEV-2014-0398; by Generalitat Valenciana, Spain, under grant PROMETEOII2014-087. G.A.G-S. acknowledges the support of CSIC and Pedeciba, Uruguay. C.A. acknowledges the support by the Spanish Government and ERDF funds from the EU Commission [Grant No. FPA2014-53631-C2-1-P] and by CONICYT Fellowship “Becas Chile” Grant No. 74150052. R.M. also thanks to COLCIENCIAS. G.A.G-S. and J.V. would like to thank Lucia Duarte for useful comments at early stages of this work.

A A2HDM contribution to V_R

Following the notation of ref. [8], we define

$$A_a = x^2 \left[((y-1)r_b^2 + 1)y - r_w^2(y-1) \right] - r_a^2(x-1), \tag{A.1}$$

$$\tilde{A}_a = A_a(r_w \rightarrow r_{H^+}), \tag{A.2}$$

$$B_a = x \left\{ [(x(y-1) + 1)r_b^2 + x - 1]y - r_a^2(y-1) \right\} - r_w^2(x-1)[x(y-1) + 1], \tag{A.3}$$

$$\tilde{B}_a = B_a(r_w \rightarrow r_{H^+}), \tag{A.4}$$

$$C_a = (x-1)(xy-1)r_b^2 - r_w^2(x-1)x(y-1) + r_a^2xy + x(y-1)(xy-1), \tag{A.5}$$

with

$$r_x \equiv \frac{m_x}{m_t}, \tag{A.6}$$

and

$$\begin{aligned}
 y_d^H &= \cos \gamma + \sin \gamma \varsigma_d, & y_u^H &= \cos \gamma + \sin \gamma \varsigma_u^*, \\
 y_d^h &= -\sin \gamma + \cos \gamma \varsigma_d, & y_u^h &= -\sin \gamma + \cos \gamma \varsigma_u^*, \\
 y_d^A &= i \varsigma_d, & y_u^A &= -i \varsigma_u^*.
 \end{aligned} \tag{A.7}$$

Then, we have the following expressions for the new contributions, listed in table 1:

– Type (1) diagrams.

$$\begin{aligned}
 I^{tHH^-} + I^{thH^-} + I^{tAH^-} &= \frac{1}{16\pi s_w^2 r_w^2} \times \\
 &\int_0^1 dx \int_0^1 dy x \left\{ \varsigma_d \left[y_u^H \sin \gamma \ln \frac{\tilde{A}_H}{\tilde{A}_A} + y_u^h \cos \gamma \ln \frac{\tilde{A}_h}{\tilde{A}_A} \right] \right. \\
 &\left. + yx \left[\frac{v_R^{uHH^+}}{\tilde{A}_H} \sin \gamma + \frac{v_R^{uhH^-}}{\tilde{A}_h} \cos \gamma - i \frac{v_R^{uAH^-}}{\tilde{A}_A} \right] \right\}, \tag{A.8}
 \end{aligned}$$

with

$$\begin{aligned}
 v_R^{u\varphi_i H^-} &= -y_u^{\varphi_i} \{ \varsigma_d [r_b^2(1-y)x + (1-x)] - \varsigma_u \} \\
 &+ y_u^{\varphi_i^*} [\varsigma_u(1-xy) - \varsigma_d], \quad \varphi_i = h, H, A. \tag{A.9}
 \end{aligned}$$

– Type (2) diagrams.

$$\begin{aligned}
 I^{bH^+H} + I^{bH^+h} + I^{bH^+A} &= -\frac{1}{16\pi s_w^2 r_w^2} \times \\
 &\int_0^1 dx \int_0^1 dy x \left\{ \varsigma_u \left[y_d^{H^*} \sin \gamma \ln \frac{\tilde{B}_H}{\tilde{B}_A} + y_d^{h^*} \cos \gamma \ln \frac{\tilde{B}_h}{\tilde{B}_A} \right] \right. \\
 &\left. + yx \left[\frac{v_R^{dH^+H}}{\tilde{B}_H} \sin \gamma + \frac{v_R^{dH^+h}}{\tilde{B}_h} \cos \gamma - i \frac{v_R^{dH^+A}}{\tilde{B}_A} \right] \right\}, \tag{A.10}
 \end{aligned}$$

with

$$\begin{aligned}
 v_R^{dH^+\varphi_i} &= -y_d^{\varphi_i} r_b^2 [\varsigma_d(1-xy) - \varsigma_u] \\
 &+ y_d^{\varphi_i^*} \{ \varsigma_u [(1-y)x r_b^2 + (1-x)] - \varsigma_d r_b^2 \}, \quad \varphi_i = h, H, A. \tag{A.11}
 \end{aligned}$$

– Type (3) diagrams.

$$\begin{aligned}
 I^{G^0tb} + I^{Htb} + I^{htb} + I^{Atb} &= \frac{1}{16\pi s_w^2} \times \\
 &\int_0^1 dx \int_0^1 dy x \left\{ x(1-x)(1-y) \left[-\frac{1}{C_Z} + \frac{y_d^{H^*} y_u^H}{C_H} + \frac{y_d^{h^*} y_u^h}{C_h} + \frac{y_d^{A^*} y_u^A}{C_A} \right] \right. \\
 &\left. - \frac{1}{r_w^2} \left[y_d^{H^*} y_u^H \ln \frac{C_H}{C_Z} + y_d^{h^*} y_u^h \ln \frac{C_h}{C_Z} + y_d^{A^*} y_u^A \ln \frac{C_A}{C_Z} \right] \right\}. \tag{A.12}
 \end{aligned}$$

– Type (6) diagrams.

$$\begin{aligned}
 I^{tG^0G^-} + I^{tHG^-} + I^{thG^-} &= \frac{1}{16\pi s_w^2 r_w^2} \times \\
 &\int_0^1 dx \int_0^1 dy x \left\{ x^2 y \left[-\frac{1+y-r_b^2(1-y)}{A_Z} + \frac{(r_b^2(y-1)+1)y_u^H - y y_u^{H*}}{A_H} \cos \gamma \right. \right. \\
 &\quad \left. \left. - \frac{(r_b^2(y-1)+1)y_u^h - y y_u^{h*}}{A_h} \sin \gamma \right] \right. \\
 &\quad \left. + y_u^H \cos \gamma \ln \frac{A_H}{A_Z} - y_u^h \sin \gamma \ln \frac{A_h}{A_Z} \right\}. \tag{A.13}
 \end{aligned}$$

– Type (7) diagrams.

$$\begin{aligned}
 I^{bG^+G^0} + I^{bG^+H} + I^{bG^+h} &= \frac{1}{16\pi s_w^2 r_w^2} \times \\
 &\int_0^1 dx \int_0^1 dy x \left\{ xy \left[\frac{1-x-r_b^2(1-x(1-2y))}{B_Z} \right. \right. \\
 &\quad \left. \left. + \frac{(r_b^2((y-1)x+1)+x-1)y_d^{H*} - xy r_b^2 y_d^H}{B_H} \cos \gamma \right. \right. \\
 &\quad \left. \left. - \frac{(r_b^2((y-1)x+1)+x-1)y_d^{h*} - xy r_b^2 y_d^h}{B_h} \sin \gamma \right] \right. \\
 &\quad \left. + y_d^{H*} \cos \gamma \ln \frac{B_H}{B_Z} - y_d^{h*} \sin \gamma \ln \frac{B_h}{B_Z} \right\}. \tag{A.14}
 \end{aligned}$$

The contribution from type (4), $\{t\varphi_i W\}$, and type (5), $\{bW\varphi_i\}$, diagrams ($\varphi_i = h, H$) is zero as in the SM:

$$V_R^{t\varphi_i W^-} = V_R^{bW^+ \varphi_i} = 0, \quad \varphi_i = h, H. \tag{A.15}$$

Notice that in the limit $s_{u,d} \rightarrow 0$, and fixing $\gamma = -\pi/2$ to identifying h with the standard Higgs, we recover the SM result [8].

Open Access. This article is distributed under the terms of the Creative Commons Attribution License ([CC-BY 4.0](https://creativecommons.org/licenses/by/4.0/)), which permits any use, distribution and reproduction in any medium, provided the original author(s) and source are credited.

References

- [1] M. Selvaggi, *Perspectives for Top quark physics at High-Luminosity LHC*, [PoS\(TOP2015\)054](#) [[arXiv:1512.04807](#)] [[INSPIRE](#)].
- [2] W. Barletta et al., *Working Group Report: Hadron Colliders*, [arXiv:1310.0290](#) [[INSPIRE](#)].
- [3] PARTICLE DATA GROUP collaboration, C. Patrignani et al., *Review of Particle Physics*, [Chin. Phys. C](#) **40** (2016) 100001 [[INSPIRE](#)].
- [4] G.A. González-Sprinberg, R. Martinez and J. Vidal, *Top quark tensor couplings*, [JHEP](#) **07** (2011) 094 [*Erratum ibid.* **05** (2013) 117] [[arXiv:1105.5601](#)] [[INSPIRE](#)].
- [5] L. Duarte, G.A. González-Sprinberg and J. Vidal, *Top quark anomalous tensor couplings in the two-Higgs-doublet models*, [JHEP](#) **11** (2013) 114 [[arXiv:1308.3652](#)] [[INSPIRE](#)].

- [6] W. Bernreuther, P. Gonzalez and M. Wiebusch, *The Top Quark Decay Vertex in Standard Model Extensions*, *Eur. Phys. J. C* **60** (2009) 197 [[arXiv:0812.1643](#)] [[INSPIRE](#)].
- [7] M. Moreno Llácer, *Search for CP violation in single top quark events with the ATLAS detector at LHC*, Ph.D. Thesis, Valencia U., IFIC (2014) [[INSPIRE](#)].
- [8] G.A. González-Sprinberg and J. Vidal, *The top quark right coupling in the tbW -vertex*, *Eur. Phys. J. C* **75** (2015) 615 [[arXiv:1510.02153](#)] [[INSPIRE](#)].
- [9] CDF collaboration, F. Abe et al., *Observation of top quark production in $\bar{p}p$ collisions*, *Phys. Rev. Lett.* **74** (1995) 2626 [[hep-ex/9503002](#)] [[INSPIRE](#)].
- [10] D0 collaboration, S. Abachi et al., *Observation of the top quark*, *Phys. Rev. Lett.* **74** (1995) 2632 [[hep-ex/9503003](#)] [[INSPIRE](#)].
- [11] C. Deterre, *W helicity and constraints on the Wtb vertex at the Tevatron*, *Nuovo Cim. C* **035N3** (2012) 125 [[arXiv:1203.6802](#)] [[INSPIRE](#)].
- [12] D0 collaboration, V.M. Abazov et al., *Search for anomalous Wtb couplings in single top quark production in $p\bar{p}$ collisions at $\sqrt{s} = 1.96$ TeV*, *Phys. Lett. B* **708** (2012) 21 [[arXiv:1110.4592](#)] [[INSPIRE](#)].
- [13] D0 collaboration, V.M. Abazov et al., *Search for anomalous Wtb couplings in single top quark production*, *Phys. Rev. Lett.* **101** (2008) 221801 [[arXiv:0807.1692](#)] [[INSPIRE](#)].
- [14] W. Bernreuther, *Top quark physics at the LHC*, *J. Phys. G* **35** (2008) 083001 [[arXiv:0805.1333](#)] [[INSPIRE](#)].
- [15] F.-P. Schilling, *Top Quark Physics at the LHC: A Review of the First Two Years*, *Int. J. Mod. Phys. A* **27** (2012) 1230016 [[arXiv:1206.4484](#)] [[INSPIRE](#)].
- [16] C. Bernardo et al., *Studying the Wtb vertex structure using recent LHC results*, *Phys. Rev. D* **90** (2014) 113007 [[arXiv:1408.7063](#)] [[INSPIRE](#)].
- [17] R. Hawkings, *Top quark physics at the LHC*, *Compt. Rendus Phys.* **16** (2015) 424.
- [18] M. Cristinziani and M. Mulders, *Top-quark physics at the Large Hadron Collider*, [arXiv:1606.00327](#) [[INSPIRE](#)].
- [19] ATLAS, CMS collaborations, *Measurements of new physics in top quark decay at LHC*, *J. Phys. Conf. Ser.* **452** (2013) 012011 [[INSPIRE](#)].
- [20] ATLAS collaboration, *Search for New Physics with Top quarks in ATLAS at 8 TeV ($t\bar{b}$, $t\bar{t}$, vector-like quarks)*, in *Proceedings, 20th International Conference on Particles and Nuclei (PANIC 14)*, Hamburg, Germany, 24–29 August 2014, pg. 579–582 [[INSPIRE](#)].
- [21] D. Bardhan, G. Bhattacharyya, D. Ghosh, M. Patra and S. Raychaudhuri, *Detailed analysis of flavor-changing decays of top quarks as a probe of new physics at the LHC*, *Phys. Rev. D* **94** (2016) 015026 [[arXiv:1601.04165](#)] [[INSPIRE](#)].
- [22] W. Bernreuther, D. Heisler and Z.-G. Si, *A set of top quark spin correlation and polarization observables for the LHC: Standard Model predictions and new physics contributions*, *JHEP* **12** (2015) 026 [[arXiv:1508.05271](#)] [[INSPIRE](#)].
- [23] J.A. Aguilar-Saavedra and J. Bernabeu, *W polarisation beyond helicity fractions in top quark decays*, *Nucl. Phys. B* **840** (2010) 349 [[arXiv:1005.5382](#)] [[INSPIRE](#)].
- [24] J. Drobnak, S. Fajfer and J.F. Kamenik, *New physics in $t \rightarrow bW$ decay at next-to-leading order in QCD*, *Phys. Rev. D* **82** (2010) 114008 [[arXiv:1010.2402](#)] [[INSPIRE](#)].

- [25] S.D. Rindani and P. Sharma, *Probing anomalous tbW couplings in single-top production using top polarization at the Large Hadron Collider*, *JHEP* **11** (2011) 082 [[arXiv:1107.2597](#)] [[INSPIRE](#)].
- [26] A. Prasath V, R.M. Godbole and S.D. Rindani, *Longitudinal top polarisation measurement and anomalous Wtb coupling*, *Eur. Phys. J. C* **75** (2015) 402 [[arXiv:1405.1264](#)] [[INSPIRE](#)].
- [27] Q.-H. Cao, B. Yan, J.-H. Yu and C. Zhang, *A General Analysis of Wtb anomalous Couplings*, [arXiv:1504.03785](#) [[INSPIRE](#)].
- [28] Z. Hioki and K. Ohkuma, *Full analysis of general non-standard tbW couplings*, *Phys. Lett. B* **752** (2016) 128 [[arXiv:1511.03437](#)] [[INSPIRE](#)].
- [29] R. Gaitan, E.A. Garces, J.H.M. de Oca and R. Martinez, *Top quark Chromoelectric and Chromomagnetic Dipole Moments in a Two Higgs Doublet Model with CP-violation*, *Phys. Rev. D* **92** (2015) 094025 [[arXiv:1505.04168](#)] [[INSPIRE](#)].
- [30] J.A. Aguilar-Saavedra, J. Carvalho, N.F. Castro, F. Veloso and A. Onofre, *Probing anomalous Wtb couplings in top pair decays*, *Eur. Phys. J. C* **50** (2007) 519 [[hep-ph/0605190](#)] [[INSPIRE](#)].
- [31] J.A. Aguilar-Saavedra, J. Carvalho, N.F. Castro, A. Onofre and F. Veloso, *ATLAS sensitivity to Wtb anomalous couplings in top quark decays*, *Eur. Phys. J. C* **53** (2008) 689 [[arXiv:0705.3041](#)] [[INSPIRE](#)].
- [32] G.L. Kane, G.A. Ladinsky and C.P. Yuan, *Using the Top Quark for Testing Standard Model Polarization and CP Predictions*, *Phys. Rev. D* **45** (1992) 124 [[INSPIRE](#)].
- [33] B. Lampe, *Forward-backward asymmetry in top quark semileptonic decay*, *Nucl. Phys. B* **454** (1995) 506 [[INSPIRE](#)].
- [34] F. del Aguila and J.A. Aguilar-Saavedra, *Precise determination of the Wtb couplings at CERN LHC*, *Phys. Rev. D* **67** (2003) 014009 [[hep-ph/0208171](#)] [[INSPIRE](#)].
- [35] M. Jezabek, *Top quark physics*, *Nucl. Phys. Proc. Suppl.* **37B** (1994) 197 [[hep-ph/9406411](#)] [[INSPIRE](#)].
- [36] M. Jezabek and J.H. Kuhn, *V-A tests through leptons from polarized top quarks*, *Phys. Lett. B* **329** (1994) 317 [[hep-ph/9403366](#)] [[INSPIRE](#)].
- [37] B. Grzadkowski and Z. Hioki, *New hints for testing anomalous top quark interactions at future linear colliders*, *Phys. Lett. B* **476** (2000) 87 [[hep-ph/9911505](#)] [[INSPIRE](#)].
- [38] R.M. Godbole, S.D. Rindani and R.K. Singh, *Lepton distribution as a probe of new physics in production and decay of the t quark and its polarization*, *JHEP* **12** (2006) 021 [[hep-ph/0605100](#)] [[INSPIRE](#)].
- [39] T. Stelzer and S. Willenbrock, *Spin correlation in top quark production at hadron colliders*, *Phys. Lett. B* **374** (1996) 169 [[hep-ph/9512292](#)] [[INSPIRE](#)].
- [40] G. Mahlon and S.J. Parke, *Angular correlations in top quark pair production and decay at hadron colliders*, *Phys. Rev. D* **53** (1996) 4886 [[hep-ph/9512264](#)] [[INSPIRE](#)].
- [41] ATLAS collaboration, *Measurement of the W boson polarization in top quark decays with the ATLAS detector*, *JHEP* **06** (2012) 088 [[arXiv:1205.2484](#)] [[INSPIRE](#)].
- [42] B. Grzadkowski and M. Misiak, *Anomalous Wtb coupling effects in the weak radiative B -meson decay*, *Phys. Rev. D* **78** (2008) 077501 [*Erratum ibid.* **D 84** (2011) 059903] [[arXiv:0802.1413](#)] [[INSPIRE](#)].
- [43] T.D. Lee, *A Theory of Spontaneous T Violation*, *Phys. Rev. D* **8** (1973) 1226 [[INSPIRE](#)].

- [44] G.C. Branco, P.M. Ferreira, L. Lavoura, M.N. Rebelo, M. Sher and J.P. Silva, *Theory and phenomenology of two-Higgs-doublet models*, *Phys. Rept.* **516** (2012) 1 [[arXiv:1106.0034](#)] [[INSPIRE](#)].
- [45] A. Pich and P. Tuzon, *Yukawa Alignment in the Two-Higgs-Doublet Model*, *Phys. Rev. D* **80** (2009) 091702 [[arXiv:0908.1554](#)] [[INSPIRE](#)].
- [46] M. Jung, A. Pich and P. Tuzon, *Charged-Higgs phenomenology in the Aligned two-Higgs-doublet model*, *JHEP* **11** (2010) 003 [[arXiv:1006.0470](#)] [[INSPIRE](#)].
- [47] M. Jung, X.-Q. Li and A. Pich, *Exclusive radiative B-meson decays within the aligned two-Higgs-doublet model*, *JHEP* **10** (2012) 063 [[arXiv:1208.1251](#)] [[INSPIRE](#)].
- [48] ATLAS, CMS collaborations, *Charged Higgs boson searches at the LHC*, *Nucl. Part. Phys. Proc.* **260** (2015) 216 [[INSPIRE](#)].
- [49] A. Celis, V. Ilisie and A. Pich, *Towards a general analysis of LHC data within two-Higgs-doublet models*, *JHEP* **12** (2013) 095 [[arXiv:1310.7941](#)] [[INSPIRE](#)].
- [50] W. Buchmüller and D. Wyler, *Effective Lagrangian Analysis of New Interactions and Flavor Conservation*, *Nucl. Phys. B* **268** (1986) 621 [[INSPIRE](#)].
- [51] J.A. Aguilar-Saavedra, *A minimal set of top anomalous couplings*, *Nucl. Phys. B* **812** (2009) 181 [[arXiv:0811.3842](#)] [[INSPIRE](#)].
- [52] CDF collaboration, T. Aaltonen et al., *Search for a Higgs Boson in the Diphoton Final State in $p\bar{p}$ Collisions at $\sqrt{s} = 1.96$ TeV*, *Phys. Rev. Lett.* **108** (2012) 011801 [[arXiv:1109.4427](#)] [[INSPIRE](#)].
- [53] D0 collaboration, V.M. Abazov et al., *Search for the standard model and a fermiophobic Higgs boson in diphoton final states*, *Phys. Rev. Lett.* **107** (2011) 151801 [[arXiv:1107.4587](#)] [[INSPIRE](#)].
- [54] LEP, DELPHI, OPAL, ALEPH, L3 collaborations, G. Abbiendi et al., *Search for Charged Higgs bosons: Combined Results Using LEP Data*, *Eur. Phys. J. C* **73** (2013) 2463 [[arXiv:1301.6065](#)] [[INSPIRE](#)].
- [55] J.F. Gunion, H.E. Haber, G.L. Kane and S. Dawson, *The Higgs Hunter's Guide*, *Front. Phys.* **80** (2000) 1 [[INSPIRE](#)].
- [56] CMS collaboration, *Search for a low-mass pseudoscalar Higgs boson produced in association with a $b\bar{b}$ pair in pp collisions at $\sqrt{s} = 8$ TeV*, *Phys. Lett. B* **758** (2016) 296 [[arXiv:1511.03610](#)] [[INSPIRE](#)].
- [57] A. Celis, V. Ilisie and A. Pich, *LHC constraints on two-Higgs doublet models*, *JHEP* **07** (2013) 053 [[arXiv:1302.4022](#)] [[INSPIRE](#)].
- [58] H.E. Haber, G.L. Kane and T. Sterling, *The Fermion Mass Scale and Possible Effects of Higgs Bosons on Experimental Observables*, *Nucl. Phys. B* **161** (1979) 493 [[INSPIRE](#)].
- [59] L.J. Hall and M.B. Wise, *Flavor changing Higgs boson couplings*, *Nucl. Phys. B* **187** (1981) 397 [[INSPIRE](#)].
- [60] J.F. Donoghue and L.F. Li, *Properties of Charged Higgs Bosons*, *Phys. Rev. D* **19** (1979) 945 [[INSPIRE](#)].
- [61] A. Arhrib and A. Jueid, *tbW Anomalous Couplings in the Two Higgs Doublet Model*, *JHEP* **08** (2016) 082 [[arXiv:1606.05270](#)] [[INSPIRE](#)].
- [62] T. Aushev et al., *Physics at Super B Factory*, [arXiv:1002.5012](#) [[INSPIRE](#)].